DOI: 10.14264/uql.2020.582

Hydraulics of Swirling Flows along Vortex Drop Shafts

G. Crispino[1], P. Contestabile[1], D. Vicinanza[1], M. Pfister[2] and C. Gisonni[1]
[1]Department of Engineering
Università degli della Campania "Luigi Vanvitelli"
Aversa, Italy
[2]Department of Civil Engineering
Haute Ecole d'Ingénierie et d'Architecture (HES-SO)
Fribourg, Switzerland
E-mail: gaetano.crispino@unicampania.it

ABSTRACT

The vortex drop shaft is a benchmark structure in hydraulic engineering. It is often used in sewers and hydropower systems, given that a significant energy dissipation combined with a reduced space occupation is achieved. Conversely, the flow pattern establishing along the structure may lead to the occurrence of unstable phenomena as vibrations, abrasion and choking, particularly if the operational conditions are different from the standard design regime. It is advantageous to study the overall hydraulic efficiency of the structure, and particularly to derive the hydraulic conditions of the swirling flow along the vertical shaft. At this regard, the paper describes a physically based approach, based on the momentum conservation, to derive the rotational angle and the velocity profiles along the shaft. The method requires the calibration of an empirical parameter accounting for the increase of the wall friction stress due to the centrifugal force. The outcomes of the application of the proposed procedure are presented with reference to the operation of two physical models of supercritical vortex drop shafts, with a tangential or a spiral inlet at the shaft top. It is shown that the application of the empirically-modified momentum approach is necessary for accounting for the significant angular momentum imparted to the swirling flow by the spiral inlet and for modelling the rotational flow distribution along the vertical shaft accurately.

Keywords: *Vortex drop shaft, energy dissipation, vortex flow, swirling flow, supercritical flow, physical model*

1. INTRODUCTION

Vortex Drop Shafts (VDSs) are hydraulic structures across which the flow dissipates a significant amount of energy and the air and water flows are separated avoiding thereby a priori choking. Their installation is frequent in urban drainage systems. There, VDSs are built to vertically connect up- and downstream sewer collectors at notably different elevations. So doing, the laying of sewers with an excessive bottom slope is avoided. The elevation difference for VDS sewer applications is typically larger than 5 to 20 m (Gisonni and Hager 2012). VDSs can also be used as flood spillways at dams (Mulligan et al. 2019). For such structures, the shaft height is considerably larger than in sewer applications.

The occurrence of rotational flows is often undesirable because of the formation of vibrations, the entrainment of air, or due to other local instability phenomena reducing the overall structure efficiency (Khatsuria 2015). Nevertheless, the recourse of VDSs being integrated in diversion structures or spillways to ensure flood control is frequent, as documented in literature (Liu et al. 2018; Zhang et al. 2018).

Early works on vortex drops were carried out by Italian hydraulicians Drioli (1947), Viparelli (1950) and Pica (1970). Several experimental studies followed and, over the years, different layouts of VDSs were proposed. The inlet device issuing the approach flow in the vertical shaft was analyzed for various geometrical configurations (circular, tangential, screw, spiral) by Drioli (1947), Laushey (1952), Jain (1984) and Kellenberger (1988). All these studies proved that the approach flow energy content is a basic parameter to design the inlet correctly. Del Giudice et al. (2010) developed an innovative solution to adapt a subcritical tangential inlet device for supercritical approach flows.

For sewer applications, a dissipation chamber is conventionally placed at the toe of the vertical shaft to reconvert the flow direction from vertical to horizontal and to de-aerate the flow. Hager and Kellenberger (1987) conceived a standard chamber configuration, and equipment in the chamber to improve the flow behavior was suggested by Del Giudice et al. (2008).

As for the vertical shaft, some design criteria to define the shaft diameter D_s are available for both sewer and spillways (Hager and Kellenberger 1987; Kellenberger 1988; Khatsuria 2015). For VDS spillways, the concern about the pressure and velocity distributions along the vertical shaft is significant since an underestimated energy

dissipation and the occurrence of cavitation can damage the shaft. Liu et al. (2018) and Zhang et al. (2018) demonstrated that turbulence models simulate the complex flow behavior in the shaft with a good accuracy. Velocity and pressure distributions along the shaft were, instead, not of a primary interest for VDSs applied in drainage systems. Zhao et al. (2006) collected flow depth and shaft wall pressure measurements in a VDS with a shaft length L_s/D_s = 12.1. Camino et al. (2015) focused on flow velocities distributions along the shaft by considering two physical models of a plunging drop shaft. Carty et al. (2019) introduced an empirical equation to derive the rotational angles in the vertical shaft. Recently, Crispino et al. (2019a, b) proposed a theoretical method based on the momentum conservation approach to derive the velocity profiles along the shaft of a VDS with L_s/D_s = 23.5. The structure operated under a supercritical approach flow regime, and the flow was directed in the vertical shaft by passing through a spiral inlet. An enhancement of this theoretical model is presented in this study. In particular, the paper aims to show that the herein discussed model schematizes the flow regime in the shaft by predicting flow angles and velocities with a good accuracy. The suggested approach is particularly applied to replicate the shaft flow behavior in two physical models of VDSs, respectively with a tangential and spiral inlet.

2. METHODOLOGY

2.1. Momentum equation

In VDSs the approach flow entering the inlet device is linear. The inlet structure deviates the flow and adds angular momentum. In the shaft, the falling flow is driven by centrifugal and gravitational forces. The center, also called "core" (Gisonni and Hager 2012), of the shaft is filled by air which escapes vertically upward through the shaft. The water flows along the shaft wall as annular flow. A sketch of an annular flow body running along the shaft is shown in Figure 1, together with a photo showing a vertical shaft in operation (Crispino et al. 2019a). As visible, the annular flow adheres to the shaft wall and the water trajectories are inclined with an angle θ relative to the horizontal. The complementary rotational angle is α. The friction due to the contact between the flow and the shaft wall generates energy dissipation. The dissipation mechanism along the vertical shaft was described by Jain (1987), who introduced a theoretical approach based on the following hypotheses:

1. the annular flow is perfectly rotation-symmetrical to the vertical axis z;
2. the tangential (subscript t) velocity distribution is assumed to be in compliance with irrotational flow. This means that the product of the tangential velocity component V_t times the radius r is constant and equal to the circulation Ω;
3. the radial velocity component is negligible and thus assumed to be zero;
4. the vertical (subscript z) velocity component does not vary over a cross-section

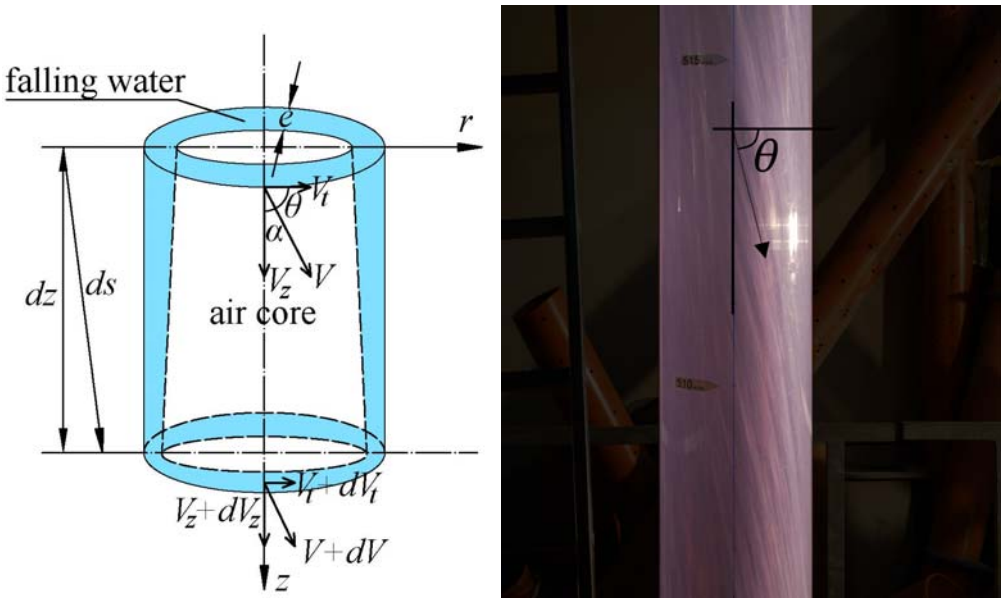

Figure 1. Definition sketch of the control volume of the annular flow (on the left) and photo of a physical model of vertical shaft in operation for an incoming discharge Q = 12.70 m^3/s (Crispino et al. 2016)

The governing equations on the flow across the control volume of height dz (Figure 1) are the continuity and the momentum equations (Jeanpierre and Lachal 1966; Jain 1987). The continuity equation is:

$$Q = A \cdot V_z \tag{1}$$

where Q is the discharge, V_z is the vertical component of the mean flow velocity and $A = \pi D_s e$ is the cross-sectional area (with an accuracy of 5% for $e/D_s < 0.05$) depending on the shaft diameter D_s and on the flow thickness e. For the control volume represented in Figure 1, the vectoral momentum equation is:

$$\rho Q\mathbf{V} - \rho Q(\mathbf{V}+\mathbf{dV}) = \pi D_s e \rho g dz - \pi D_s \boldsymbol{\tau} ds \tag{2}$$

where vectors $\rho Q\mathbf{V}$ and $\rho Q(\mathbf{V}+\mathbf{dV})$ are the entering and outing momentum fluxes, with ρ as the water density, $\pi D_s e \rho g dz$ is the weight of the fluid volume, with g as the gravity acceleration, and $\boldsymbol{\tau}\pi D_s ds$ is the frictional force due to the shear stress $\boldsymbol{\tau}$ acting on the ds-long surface (Figure 1). The centrifugal forces inducing pressure on the shaft wall should be theoretically included in Eq. (2). However, in the present approach the pressure forces were ignored since the flow tickness e is small.
Eq. (2) can be formulated for the vertical and horizontal (tangential) component as $V_z = V\cos\alpha$ and $V_t = V\sin\alpha$ (Figure 1):

$$\rho Q V \cos\alpha - \rho Q (V+dV)\cos(\alpha+d\alpha) = \pi D_s e \rho g dz - \tau \pi D_s dz \cos\alpha \tag{3}$$

$$\rho Q V \sin\alpha - \rho Q (V+dV)\sin(\alpha+d\alpha) = -\tau \pi D_s dz \sin\alpha \tag{4}$$

Eq. (1) can be substituted in Eqs. (3) and (4) to obtain:

$$\rho\, \pi D_s e V_z\, V \cos\alpha - \rho\, \pi D_s e V_z\, (V+dV)\cos(\alpha+d\alpha) = \pi D_s e \rho g dz - \tau \pi D_s dz \cos\alpha \tag{5}$$

$$\rho\, \pi D_s e V_z\, V \sin\alpha - \rho\, \pi D_s e V_z\, (V+dV)\sin(\alpha+d\alpha) = -\tau \pi D_s dz \sin\alpha \tag{6}$$

Eqs. (5) and (6) can be further simplified by developing a Taylor series of $\cos(\alpha+d\alpha)$ and $\text{sen}(\alpha+d\alpha)$ in which lower terms can be neglected. This leads to:

$$\rho\, \pi D_s e V_z\, d(V\cos\alpha) = \pi D_s e \rho g dz - \tau \pi D_s dz \cos\alpha \tag{7}$$

$$\rho\, \pi D_s e V_z\, d(V\,\text{sen}\alpha) = -\tau \pi D_s dz\, \text{sen}\alpha \tag{8}$$

Given the wall shear stress $\tau = \lambda/4 \cdot \rho \cdot V^2/2$, with λ as the friction factor, Eqs. (7) and (8) can be finally written as:

$$d(V_z^2/2g) = [1 - \lambda/(4eg)\cdot V^2/2\cos\alpha]\, dz \tag{9}$$

$$d(V_t^2/2g) = -[(1-\cos^2\alpha)/\cos\alpha\ \lambda/(4eg)\cdot V^2/2]\, dz \tag{10}$$

Eqs. (9) and (10) are thus useful to derive vertical and tangential velocity profiles. As described by Crispino et al. (2019a), these equations can be discretized giving:

$$V_{z,2} = \{[1 - \lambda/(4e_1 g)\cdot V_1^2/2\cos\alpha_1]\, \Delta z_{1,2} + V_{z,1}^2/2\}^{0.5} \tag{11}$$

$$V_{t,2} = \{-[(1-\cos^2\alpha_1)/\cos\alpha_1\ \lambda/(4e_1 g)\cdot V_1^2/2]\, \Delta z_{1,2} + V_{t,1}^2/2\}^{0.5} \tag{12}$$

where subscripts 1 and 2 refer to two consecutive horizontal cross-sections with a vertical distance $\Delta z_{1,2}$.
These equations can be solved by supposing two boundary conditions. The computation procedure starts at the shaft inlet ($z = 0.0$ m) where the total discharge Q is given. The second boundary condition is usually assigned to V by using the free vortex theory to model the velocity distribution along the inlet, which initiates the approach flow rotation.

2.2. Experimental data

The abovementioned theoretical model is applied to derive the velocity profiles along the vertical shaft of VDSs headed by tangential and spiral inlets (Figure 2). The experimental data collected by Zhao et al. (2006) and Crispino et al. (2019a) are considered.

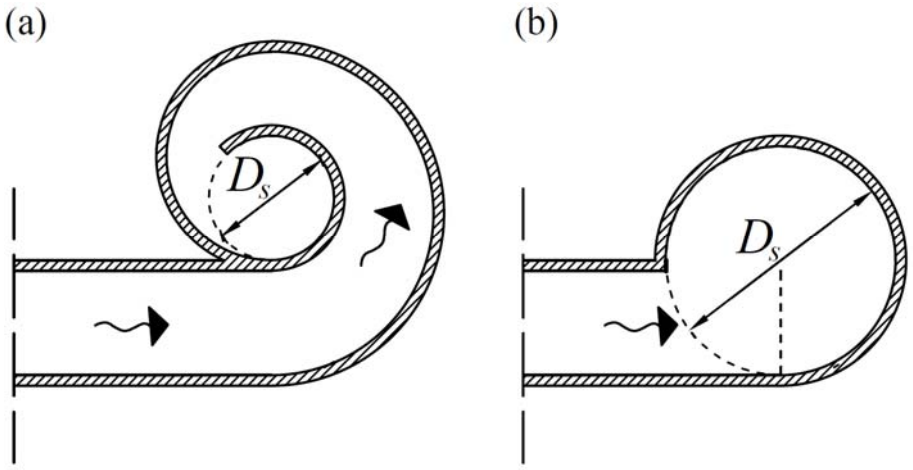

Figure 2. sketch of: (a) spiral inlet; (b) tangential vortex inlet

Zhao et al. (2006) studied a vortex drop structure with a tangential-typed inlet (Quick 1990), with a first outer radius R = 0.16 m, at the top of the vertical shaft (D_s = 0.223 m and L_s = 2.70 m). Some experimental tests were conducted with a supercritical approach flow in a rectangular channel. Velocity components were derived from the measurements of the shaft wall pressure, whereas e was measured using a specially designed small L-shaped probe. The main hydraulic features of the tests performed by Zhao et al. (2006) are resumed in the Table 1, where subscripts o and in are referring to the tangential inlet cross-section and to the shaft inlet cross-section. Table 1 also reports the approach Froude number $\mathsf{F}_o = V_o/(gh_o)^{0.5}$, with h as flow depth, the capacity Froude number relative to the vertical shaft $\mathsf{F}_C = Q/(g{\cdot}D_s^5)^{0.5}$ and the mean velocity of the flow at the shaft entrance V_{in} derived by applying the free-vortex distribution theory (Quick 1990) as

$$V_{in} = V_o{\cdot}R/(D_s/2 - e_{in}) \tag{13}$$

Table 1. Hydraulic features of the test performed by Zhao et al. (2006)

Q	F_o	F_C	V_o	V_{in}	e_{in}
0.051 m^3/s	3.50	0.69	3.92 m/s	8.79 m/s	0.031 m

Crispino et al. (2019a,b) conducted an experimental campaign on a supercritical VDS controlled by a spiral inlet chamber. The vertical shaft model was characterized by a diameter D_s = 0.31 m and a length L_s = 7.22 m, and the spiral inlet had a first radius R = 0.43 m. Selected tests (Table 2), with F_C ranging between 0.09 and 0.56, are considered herein. During each test, the rotational flow angles of the streamlines along the shaft were measured. The approach velocity V_o was measured with a micro-propeller (±1%), and V_{in} was derived by using the free-vortex theory as indicated by Crispino et al. (2019a). The flow thickness e_{in} is, instead, calculated by using Eq. (1) as a function of Q and of the vertical velocity component $V_{in,z} = V_{in}{\cdot}\cos\theta_s$. where θ_s = 30° is the spiral bottom slope.

Table 2. Hydraulic features of the tests performed by Crispino et al. (2019a)

Q	F_o	F_C	V_o	V_{in}	e_{in}
0.015 m^3/s	6.29	0.09	2.44 m/s	6.91 m/s	0.013 m
0.038 m^3/s	3.36	0.34	2.59 m/s	7.34 m/s	0.045 m
0.074 m^3/s	2.50	0.46	2.70 m/s	7.64 m/s	0.057 m
0.092 m^3/s	2.36	0.56	2.55 m/s	7.23 m/s	0.075 m

2.3. Shaft flow regime

According to Eqs. (11) and (12), the velocity profiles are obtainable by defining the shaft friction factor λ. This was estimated by using the Moody's diagram (Figure 3) as a function of the Reynolds number $\mathsf{R} = 4 \cdot R_h \cdot V_{in}/\nu$, with $R_h = e_{in} \cdot (2 - e_{in}) \cdot D/4$ as the hydraulic radius and ν as the water kinematic viscosity, and of the relative shaft wall roughness ε. The latter was in the turbulent smooth regime for both physical models of Zhao et al. (2006) and Crispino et al. (2019a, Figure 3). For this reason, in the next applications λ is computed by using the following equation suggested by Zigrang and Sylvester (1985):

$$\lambda = 0.25 \cdot [\log(\varepsilon/3.7 + 13/\mathsf{R})]^{-2} \tag{14}$$

Eq. (14) approximates the calculation of the friction factor by about 2%, as stated by Gisonni and Hager (2012). On the other hand, this relation allows to derive explicitly λ.

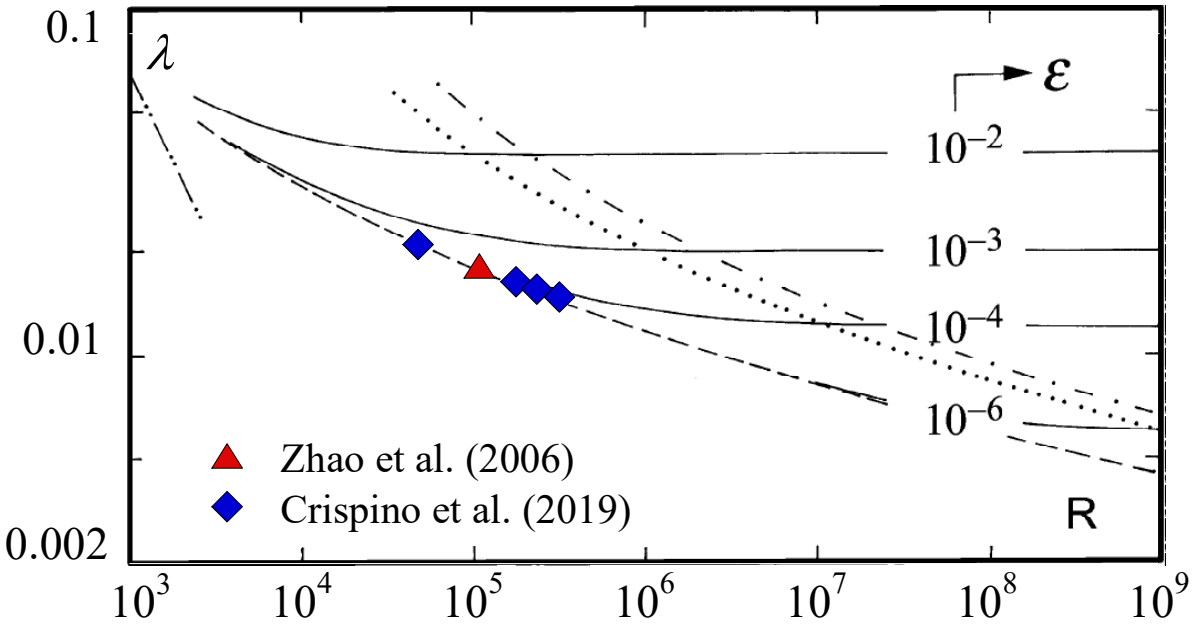

Figure 3. Moody-diagram with indication of the shaft flow regime for tests carried out by Zhao et al. (2006) and Crispino et al. (2019a)

3. RESULTS

3.1. Standard momentum equation

Eqs. (11) and (12) give the vertical and tangential velocity components V_z and V_t, and consequently the mean velocity V. It is thus possible to derive α as:

$$\alpha = \arctan(V_t/V_z) \tag{15}$$

The results of the combined application of Eqs. (1), (11), (12) and (15) are compared to the observations of Zhao et al. (2006) and Crispino et al. (2019a) in Figures 4 and 5.

Figure 4 shows that the computed values of e, V_z and V_t are in a good agreement with the measurements collected by Zhao et al. (2006). The relative error in the calculation of the velocity components is equal to about 10%, whereas e is computed by a mean relative error of about 14%. It is noteworthy that the momentum approach gives vertical velocity values larger than the corresponding observations whereas the predicted tangential velocities are slightly smaller than the observed ones.

In the Figure 5 a comparison between the computed and measured α for the tests with $\mathsf{F}_C = 0.09$ and $\mathsf{F}_C = 0.56$ is shown.

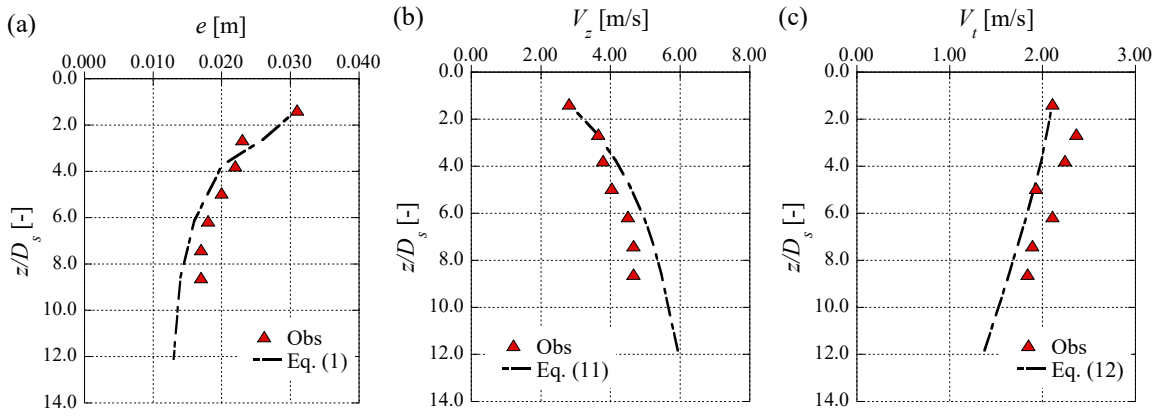

Figure 4. Comparison between observations (Obs) and predictions (see section 2.1) for the VDS of Zhao et al. (2006): (a) e; (b) V_z; (c) V_t

For F_C = 0.09 (Figure 5a) the discrepancies between measurements and predictions are not negligible, with a relative error of about 40%. If F_C increases (Figure 5b), then the theoretical approach significantly overestimates α. This means that the momentum balance equations, as conceived in the section 2.1, tend to underestimate the flow friction mechanism along the shaft and to excess the flow rotation. The larger Q (or F_C) is the more significant becomes the error in the prediction of α. This is probably related to the ideal assumption of the axisymmetric and irrotational flow across the vertical shaft (see section 2.1). On the other hand, the centrifugal forces become presumably relevant when augmenting Q, and correspondingly F_C. Zhao et al. (2006) stated that the forces giving a pressure on the shaft wall are significant at the drop shaft entrance, where the flow thickness gradient is large, whereas they can be neglected for small values of e, that are typically observed along most of the shaft length. According to the present results, this simplification is acceptable when e is small, whereas the imprecision of the momentum conservation approach results to be intolerable in the first part of the shaft, where the centrifugal effect due to the spiral inlet is more relevant.

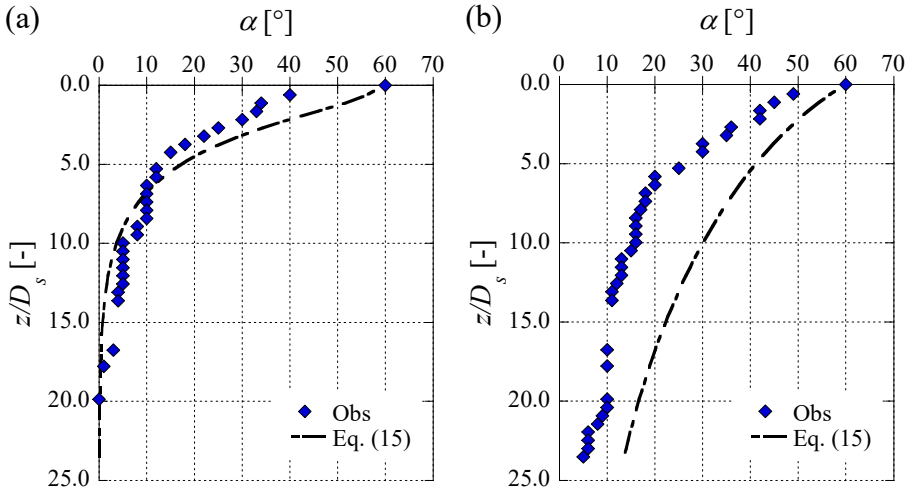

Figure 5. Comparison between observed (Obs) and computed (Eq. 15) α in the VDS of Crispino et al. (2019a): (a) F_C = 0.09; (b) F_C = 0.56

As compared to the flow observations of Crispino et al. (2019a), the centrifugal forces in the upper part of the vertical shaft considered by Zhao et al. (2006) are not so relevant to make the shaft flow features not accurately predictable by the momentum approach. This can be attributed to the approach flow rotation induced by the tangential-typed inlet. The wall of the tangential inlet forces the approach flow to complete a 270°-rotation leaving an open 90°-slot (Quick 1990). Conversely, in the spiral inlet of Crispino et al. (2019a), the flow adhered to the wall of the spiral and it concluded a rotation of 585°. The centrifugal effect induced by the spiral was thus more considerable than that one generated by the passage of the approach flow along the tangential inlet.

For this reason, the momentum approach, as presented in the previous section, is appropriate to predict the hydraulic features of the swirling flow issued by a tangential inlet across the vertical shaft. Conversely, according to the present experimental data the computation procedure based on the set of Eqs. (1), (11), (12) and (15) is not adequate to calculate the velocity profiles along the vertical shaft with a spiral inlet at its top.

3.2. Assumption of a friction increase

To adapt the standard momentum equation predicting the flow rotational angles along the vertical shaft headed by the spiral inlet, λ is here multiplied with a n-parameter. Eqs. (11) and (12) are thereby converted in:

$$V_{z,2} = \{[1 - n \cdot \lambda/(4e_1 g) \cdot V_1^2/2 \cos\alpha_1] \Delta z_{1,2} + V_{z,1}^2/2\}^{0.5} \quad (16)$$

$$V_{t,2} = \{- [(1 - \cos^2\alpha_1)/\cos\alpha_1 \, n \cdot \lambda/(4e_1 g) \cdot V_1^2/2] \Delta z_{1,2} + V_{t,1}^2/2\}^{0.5} \quad (17)$$

Crispino et al. (2019a) suggested to use a constant value of n along the shaft to be calculated as $n = 10 \cdot F_c$. The results derived by the application of the constant value of n in the momentum equations are shown in Figure 6 for $F_C = 0.09$ (Figure 6a) and $F_C = 0.56$ (Figure 6b). As compared to Figure 5, it is evident that the accuracy of the momentum balance approach in predicting α is now sensibly improved, especially for $F_C = 0.56$. The mean relative error is about 40% for all the tests of Table 2. α is still overestimated in the first part of the shaft, indicatively up to $z/D_s = 7.0$. Further down, the model gives smaller angles than the observed ones. Under a design perspective, it would be more convenient to overestimate α because the assumption of a zero rotation at the shaft end corresponds to the achievement of quasi-uniform flow conditions and, consequently, to an erroneous definition of the flow conditions at the shaft outlet.

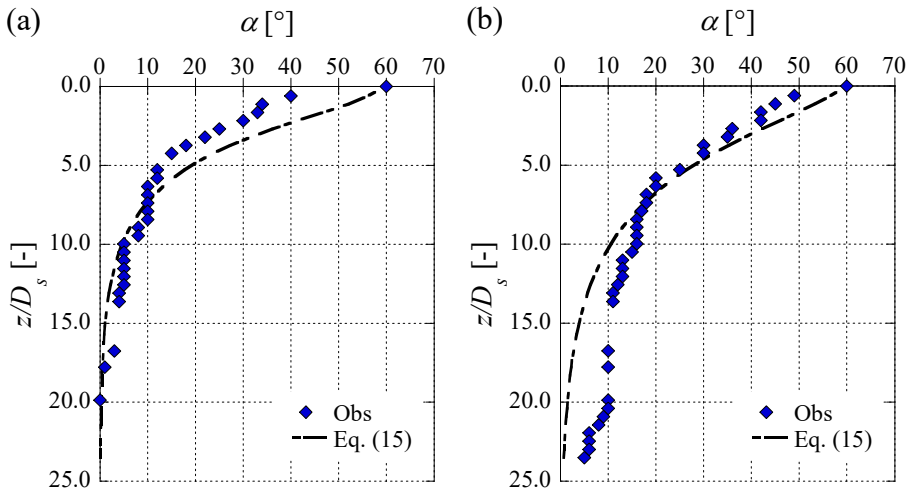

Figure 6. Comparison between observed (Obs) and computed (Eq. 15) α in the VDS of Crispino et al. (2019a), with the introduction of $n = 10 \cdot F_c$: (a) $F_C = 0.09$; (b) $F_C = 0.56$

A new calculation of the corrective n-parameter is proposed in the present paper. The effect of the centrifugal forces on the swirling flow is more significant along the first part of the shaft, where the rotational motion dissipates more rapidly following Crispino et al. (2019a). The value n is mainly decisive along this upper shaft part. At this aim, the n-parameter can be set equal to:

$$n = 15 \cdot F_C \quad (18)$$

for $z/D_s \leq 5.0$, or to:

$$n = 5 \cdot F_C \cdot e^{-0.20 \cdot z/D_s} \quad (19)$$

for $z/D_s > 5.0$. The results derived by using Eqs. (18) and (19) for calculating the n-parameter are represented in Figure 7 for all the tests resumed in Table 2. The measured α values fit then by the momentum approach, given that the relative error reduces to 25 %. According to Eqs. (18) and (19), n-parameter is not dependent on the shaft depth z along the upper shaft part ($z/D_s \leq 5.0$), and then it rapidly decays as the flow falls down $z/D_s > 5.0$. This is also coherent with the experimental observations of Carty et al. (2019) who analyzed the streamline flow regime along the vertical shaft of VDSs. In particular, Carty et al. (2019) showed that the falling flow could be assumed as fully irrotational for $z/D_s \leq 5.0$, giving a circulation constant along the upper shaft part. Centrifugal effects do not vary with z in this shaft region, and this observation sustains the assumption of a constant amplifying factor for $z/D_s \leq 5.0$ as Eq. (18) gives. Downstream of $z/D_s = 5.0$, instead, Carty et al. (2019) observed a free-surface and velocity profiles of the annular jet more uniform, allowing to assume that α decreases along the shaft according to a power curve as:

$$\alpha = 32.94 \cdot z^{-0.735} - 10 \quad (20)$$

A non-linear relation between α and z was thus also derived by Carty et al. (2019), as recommended by using Eq. (19). On the other hand, the effect of the increase of Q (or F_C) is not modelled in Eq. (20) despite its relevance. At this regard, Figure 8 demonstrates that the error made by using Eq. (20) to estimate the distribution of α is larger as F_C increases. This proves that an accurate empirical recommendation to predict α along vertical shafts must keep into account that centrifugal effects are more significant by augmenting F_C.

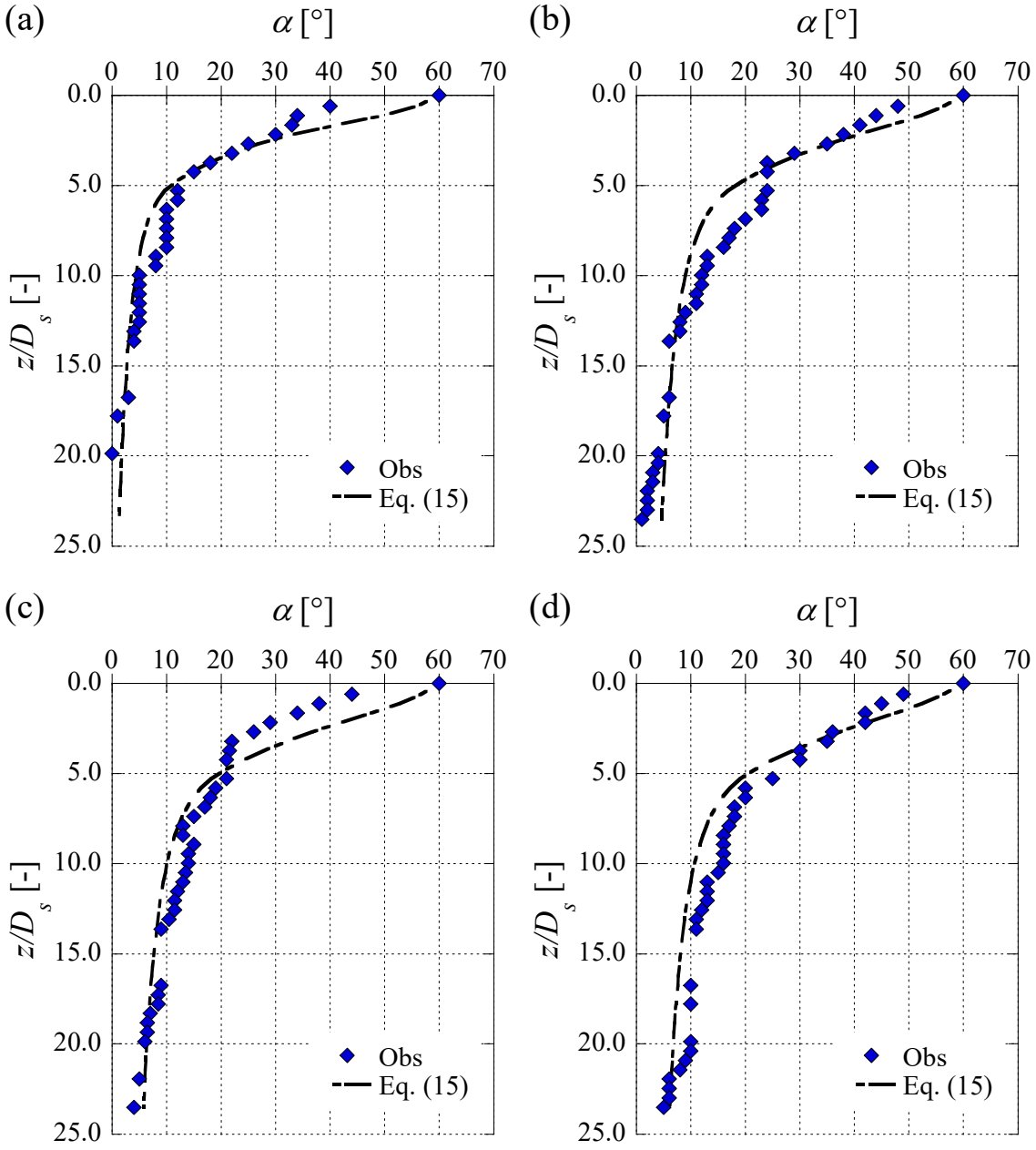

Figure 7. Comparison between observed (Obs) and computed (Eq. 15) α in the VDS of Crispino et al. (2019a), with the introduction of n derived by Eqs. (18) and (19): (a) $F_C = 0.09$; (b) $F_C = 0.34$; (c) $F_C = 0.46$; (d) $F_C = 0.56$

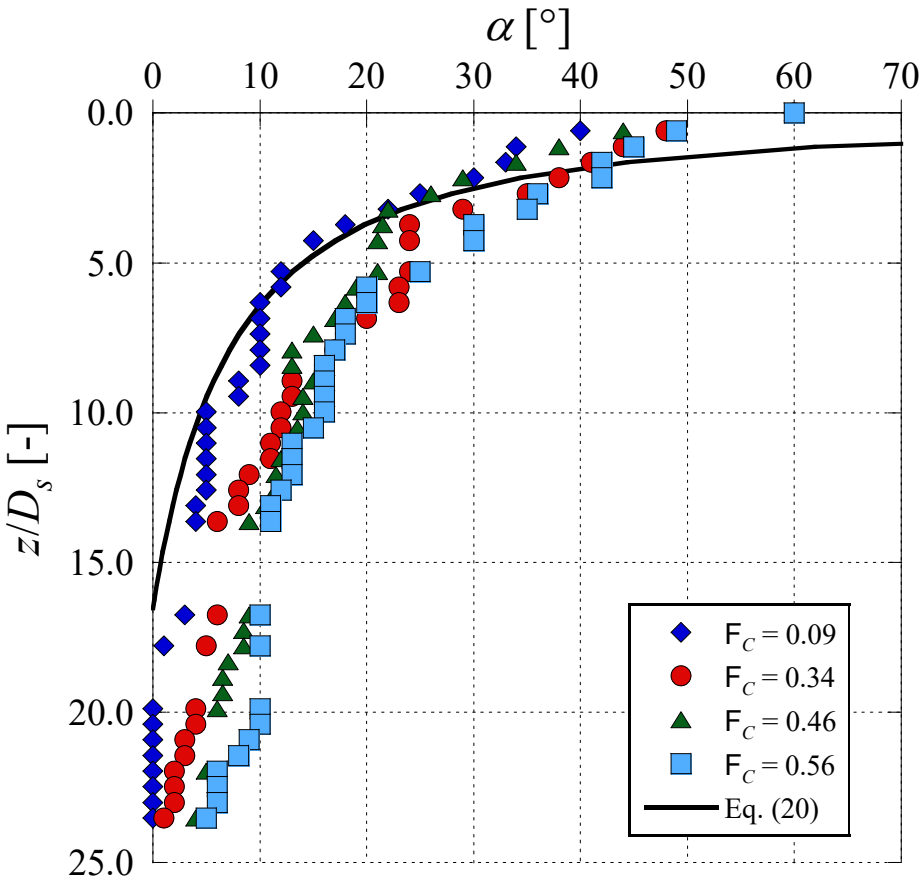

Figure 8. Comparison between observed (Obs) and computed (Eq. 20) α in the VDS of Crispino et al. (2019a)

4. CONCLUSIONS

The theoretical formulation of a swirling flow along vertical shafts of vortex drop structures is assessed. A prediction of the shaft flow features is required when vortex drop shafts have to be designed or validated. The selection of the appropriate shaft material and dimensions, on one hand, and the verification of the energy dissipation, on the other one, requires a reliable prediction of velocities, rotational angles, and pressures across the shaft.

Early studies on drop shaft hydraulics suggested to apply the momentum equation, together with the continuity, to derive flow velocities, wall pressures and flow thickness. As shown herein, this traditional approach works well for vortex drop shafts with tangential inlets. If the vertical shaft is controlled by a spiral inlet, then the present results indicate that significant centrifugal effect along the upper part of shaft de-equilibrates the momentum balance. Then, the introduction of an empirical n-parameter to consider the implicit increase of the shaft wall roughness is necessary. The results show that such shaft friction factor n is quite reliable. An enrichment of the experimental dataset of vortex drop shafts with spiral inlet will be desirable to further test the accuracy of the present computational approach.

5. REFERENCES

Camino, G. A., Zhu, D. Z., and Rajaratnam, N. (2014). Flow Observations in Tall Plunging Flow Dropshafts. *J. Hydraul. Eng.*, 141(1), 06014020.

Carty, A., O'Neill, C., Nash, S., Clifford, E., and Mulligan, S. (2019). Hydrodynamic Modelling Approaches to Assess Mechanisms Affecting the Structural Performance and Maintenance of Vortex Drops Shaft Structures. *J. Struct. Integrity Maint.*, 4(3), 162–178.

Crispino, G., Dorthe, D., Fuchsmann, T., Gisonni, C., and Pfister, M. (2016). Junction Chamber at Vortex Drop Shaft: Case Study of Cossonay. *Proc., Hydraulic Structures and Water System Management*, Utah State University, Logan, UT, 437–446.

Crispino, G., Pfister, M., and Gisonni, C. (2019a). Hydraulic Design Aspects for Supercritical Flow in Vortex Drop Shafts. *Proc., Urban Water J.*, 16(3), 225-234.

Crispino, G., Ribi, J. M., Pfister, M., and Gisonni, C. (2019b). Hydraulics of a Physical Model of Supercritical Vortex Drop Shaft. *Proc., 38th IAHR World Congress – Water Connecting the World*, IAHR, Madrid, Spain, 2444–2452.

Del Giudice, G., Gisonni, C., and Rasulo, G. (2008). Vortex Shaft Outlet. *Advances in Water Resources and Hydraulic Engineering,* Tsinghua University Press*,* Beijing*,* 2053–2058.

Del Giudice, G., Gisonni, C., and Rasulo, G. (2010). Design of a Scroll Vortex Inlet for Supercritical Approach Flow. *J. Hydraul. Eng.*, 136(10), 837–841.

Drioli, C. (1947). Su un Particolare Tipo di Imbocco per Pozzi di Scarico. *Energ. Elettr*, 24(10), 447–452.

Gisonni, C., and Hager, W. H. (2012). Idraulica dei Sistemi Fognari – dalla Teoria alla Pratica, Springer-Verlag, *Milan*.

Hager, W. H., and Kellenberger, M. H. (1987). Die Dimensionierung des Wirbelfallschachtes. *gwf - Wasser/Abwasser*, 128(11), 585–590.

Jain, S. C. (1984). Tangential vortex-inlet. *J. Hydraul. Eng.*, 110(12), 1693–1699.

Jeanpierre, D., and Lachal, A. (1966). Dissipation D'energie dans un Puits a Vortex. *La Houille Blanche*, 7, 823–832.

Kellenberger, M. H. (1988). Wirbelfallschächte in der kanalisationstechnik." VAW-Mitteilung 98, ETH, *Zurich*.

Khatsuria, R. M. (2005). Hydraulics of Spillways and Energy Dissipators, Marcel Dekker, *New York.*

Laushey, L. M. (1952). Flow in Vertical Shafts. Carnegie Institute of Technology, Department of Civil Engineering, Pittsburgh, Pa.

Liu, Z. P., Guo, X. L., Xia, Q. F., Fu, H., Wang, T., and Dong, X. L. (2018). Experimental and Numerical Investigation of Flow in a Newly Developed Vortex Drop Shaft Spillway. *J. Hydraul. Eng.,* 144(5), 04018014.

Mulligan, S., Plant, J., Nash, S., and Clifford, E. (2019). Vortex Drop Shaft Structures: State-Of-The-Art and Future Trends. *Proc., 38th IAHR World Congress – Water Connecting the World*, IAHR, Madrid, Spain, 3860–3869.

Pica, M. (1970). Scaricatori a Vortice. *Energ. Elettr*, 47(4), 217-234.

Pfister, M., Crispino, G., Fuchsmann, T., Ribi, J. M., and Gisonni, C. (2016). Multiple Inflow Branches at Supercritical-type Vortex Drop Shaft. *J. Hydraul. Eng.*, 144(11), 05018008.

Quick, M.C. (1990). Analysis of spiral vortex and vertical slot vortex drop shafts. *J. Hydraul. Eng.*, 116(3), 309–325.

Viparelli, M. (1950). Su un Particolare Tipo d'imbocco e sull'Efflusso con Vortice. *Energ. Elettr*, 27(10), 610-621.

Zhang, W., Wang, J., Zhou, C., Dong, Z., and Zhou, Z. (2018). Numerical Simulation of Hydraulic Characteristics in a Vortex Drop Shaft. *Water-Sui,* 10(1), 1393.

Zhao, C. H., Zhu, D. Z., Sun, S. K., and Liu, Z. P. (2006). Experimental Study of Flow in a Vortex Drop Shaft. *J. Hydraul. Eng.*, 132(1), 61–68.

Zigrang, D. J. and Sylvester, N .D. (1985). A Review Of Explicit Friction Factor Equations. *J. Energy Resour. Technol.*, 107, 280–283.